




# Enhanced microwave absorption properties of polymer-derived SiC/SiCN composite ceramics modified by TiC

Xiaoling Liu<sup>1,2</sup> , Zhiming Tang<sup>1</sup>, Jimei Xue<sup>1,\*</sup>, Hanjun Wei<sup>1</sup>, Xiaomeng Fan<sup>1</sup>, Yongsheng Liu<sup>1,\*</sup>, and Laifei Cheng<sup>1</sup>

<sup>1</sup> Science and Technology on Thermostructure Composite Materials Laboratory, Northwestern Polytechnical University, West Youyi Rd., No. 127, Xi'an 710072, Shaanxi, People's Republic of China

<sup>2</sup> Xi'an ASN Technology Group Co., Ltd, Xi'an 710065, Shaanxi, People's Republic of China

**Received:** 23 November 2020

**Accepted:** 24 December 2020

**Published online:**  
12 January 2021

© The Author(s), under exclusive licence to Springer Science+Business Media, LLC part of Springer Nature 2021, corrected publication 2021

## ABSTRACT

Porous SiCN(Ti) composite ceramics with good microwave absorbing performance were fabricated by pyrolysis of solid polysilazane modified by tetrabutyl titanate. The introduction of Ti not only acted as active filler to react with free carbon in the matrix to form TiC, but also played the role as catalyst to promote the formation of SiC nanowires. Finally, SiCN(Ti) composite ceramics formed a microstructure containing multi-nanophases and multi-nano heterogeneous interfaces when annealing temperature reached 1500 °C. The complex microstructure annealed at 1500 °C made composite ceramics have good matching impedance, as well as greatly increase the interfacial polarization loss and dipole polarization loss. As a result, the TiC/SiC/SiCN composite ceramics showed the excellent performance of electromagnetic wave absorption in X band. The minimum reflection loss (RL) of samples was -17.1 dB at the thickness of 1.9 mm, and the maximum effective absorption bandwidth (EAB) of composite ceramics was 3.2 GHz when the thickness of sample was 2.1 mm, which exhibited a promising prospect as a structural and microwave absorbing integration material.

## 1 Introduction

With the rapid development of microwave technology, microwave technology has penetrated many aspects of our life, such as radar, wireless

communication, meteorological, and astronomical observation, medical technology and so on [1, 2]. It has become an indispensable technology to improve our life. However, electromagnetic (EM) microwave permeated in the air will also cause electromagnetic pollution, which will inevitably bring adverse effects

Xiaoling Liu and Zhiming Tang are co-first authors; they contributed equally to the work.

Address correspondence to E-mail: xm2006caihua@163.com; yongshengliu@nwpu.edu.cn

on our lives [3]. So the application of absorbing material has become a very effective means to reduce electromagnetic pollution. Compared with traditional microwave absorbing material, such as metal and conductive polymer material, ceramics are more suitable for use as structural and microwave absorbing integration materials in harsh environment. Especially, due to its low ceramic conversion temperature and microstructure designability, the way of polymer-derived ceramics (PDCs) has received more attention than traditional technology to produce ceramics recently.

Because of excellent performance at high temperature, polymer-derived silicon-based ceramics have been studied and applied in ceramics matrix composites in recent years [4]. In particular, polymer-derived silicon carbonitride (SiCN) ceramic, which combines the properties of advanced engineering SiC and  $\text{Si}_3\text{N}_4$  ceramics, makes it possess high hardness, outstanding high temperature stability, good oxidation, and creep resistance. Meanwhile, after proper thermal treatments, PDCs-SiCN can have tailored chemical composition and show abundant nano-microstructure phases, which leads to its good microwave absorption performance [5–8]. However, in order to obtain the good microwave absorbing properties, PDCs-SiCN needs to be annealed at high temperature which will damage the fibers and is not conducive to the preparation of high-performance ceramics matrix composites. At present, there are usually two ways to improve microwave absorption properties of PDCs at relatively low heat treatment temperature. The introduction of electrically conductive phase into PDCs is a very effective method to enhance electromagnetic wave loss [9–11]. Duan successfully prepared the PDCs-SiOC composite ceramics modified by nano-SiC particles [12]. The addition of nano-SiC particles in SiOC composite ceramics boosts the in situ precipitation of nanophases (such as nano-SiC grains and free carbon) from the matrix. The minimum RL and EAB of SiOC ceramics modified by nano-SiC reaches  $-61$  dB and 3.5 GHz in X band because of abundant nanophases formed in matrix. Han fabricated the porous PDCs-SiOC composite ceramics with hierarchical microstructure of graphene and SiC nanowires by polymer pyrolysis process [13]. The unique one-dimensional and two-dimensional coexisting microstructure in matrix makes the minimum RL and maximum EAB attain  $-69.3$  dB and 3.9 GHz,

respectively. However, this method also has obvious limitation. The electrically conductive phase is easy to agglomerate and difficult to evenly distribute in matrix. Another effective way to enhance microwave absorption properties of PDCs is to add catalyst in precursor. One-dimensional nanostructure of conductive phase can be uniformly dispersed in PDCs via pyrolysis of the polymeric precursor containing catalyst. Unique microstructure and large specific surface area of one-dimensional conductive phase can easily form conductive networks and increase surface polarization, which can greatly attenuate propagation of electromagnetic microwave in matrix [14–18]. Meanwhile, there are some researches to indicate that permittivity gradient formed in composite ceramics between phase composition is very conducive to the improvement of microwave absorption properties. Kong synthesized ZnO/ $\text{ZnAl}_2\text{O}_4$ /paraffin composite material via sol-gel process [19]. Paraffin is used as electromagnetic transparent phase and is denoted as A phase.  $\text{ZnAl}_2\text{O}_4$  and ZnO are called B and C phases and as high and low electrical lossy phases, respectively. Due to appropriate permittivity gradient, the minimum RL of composite material reaches  $-25$  dB, and EAB expands the whole X band.

The present work focuses on fabrication of PDCs-SiCN composite ceramics modified by TiC. On one hand, Ti introduced in PDCs-SiCN composite ceramics acts as catalyst to promote the precipitation of SiC. On the other hand, conductive TiC generated during the heat treatment can increase conductivity loss and form permittivity gradient with SiC to improve the interface polarization loss. The microstructure evolution of TiC/SiC/SiCN composite ceramics with annealing temperature was characterized. The formation mechanisms of SiC nanowires (NWs) and TiC were discussed. Dielectric properties and microwave absorption performance of composite ceramics in X band (8 ~ 12 GHz) were analyzed.

## 2 Experimental procedure

### 2.1 Material fabrication

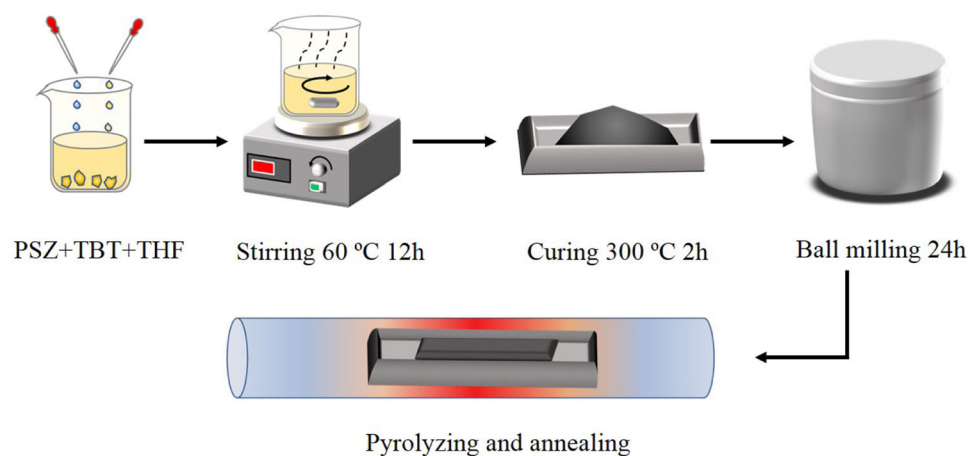
The commercial solid polysilazane (PSZ) was supplied by Hangzhou Aisen new material technology co., Ltd and used as pre-ceramics precursor.

Tetrabutyl titanate (TBT) and tetrahydrofuran (THF) were purchased from Aladdin company, and their purity were all analytic grade without further purification. Figure 1 shows the schematic diagram of main preparation process of composite ceramics. Firstly, TBT and PSZ were dissolved in the THF to form homogenous solution with 5 wt% and 95 wt%, respectively. The mixed solution was stirred at 60 °C for 12 hours until the THF in solution volatilized completely, and the PSZ precursor modified by Ti was obtained. Previous researches indicate that the condensation reaction between Si-H bond of precursor and butoxy group in TBT occurs during the mixing process, which leads to formation of the precursor including the Si-O-Ti bonds [20, 21]. The introduced Ti atoms were uniformly distributed in the precursor at atomic level. The dried PSZ precursor including Ti was cross-linked and cured at 300 °C for 2 hours under the protection of Ar atmosphere. Then cross-linked precursor was ball milled for 24 hours at 300 r/min, and the powder was sieved with 200-mesh sieve. Subsequently, the uniform powder was cold-pressed into strip green bodies with the size of  $4 \times 15 \times 70 \text{ mm}^3$  under the pressure of 20 MPa. Finally, the green bodies were pyrolyzed at 900 °C for 2 hours and then annealed at 1300 °C, 1400 °C, and 1500 °C, respectively. The pyrolysis and heat treatment were all protected under the Ar atmosphere.

## 2.2 Material characterization

The thermogravimetric (TG) and differential scanning calorimetry (DSC) curves of modified powder were obtained with STA-499-F3. The X'Pert Pro Multipurpose Powder Diffractometer with Cu  $K\alpha$  radiation (Philips, Eindhoven, Netherlands) was

**Fig. 1** Schematic illustration of the fabrication of TiC/SiC/SiCN composite ceramics



used to analyze the phases composition of TiC/SiC/SiCN composite ceramics. The transmission electron microscopy (TEM, G-20, FEI-Tecnai, 300 kV, Hillsboro, USA) and scanning electron microscope (SEM, S-4700, Hitachi, Tokyo, Japan) were employed to observe the microstructure and morphology of samples. Carbon phase in composite ceramics was detected and analyzed by Raman spectrum analyzer (RMS, Renishaw, UK).

The complex permittivities of composite ceramics were measured by using the vector network analyzer (Anritsu MS4644A, Japan) with waveguide method. The reflection loss (RL) of sample was calculated according to Eq. (1) ~ (2) based on the metal back panel model and transmission line theory.

$$RL(dB) = 20 \bullet \log_{10} |(Z_{in} - 1)/(Z_{in} + 1)| \quad (1)$$

$$Z_{in} = \sqrt{\frac{\mu}{\epsilon}} \tanh(j2\pi\sqrt{\mu\epsilon}fd/c) \quad (2)$$

where the  $\epsilon$  and  $\mu$  are the relative permittivity and permeability of samples, respectively. Because the composite ceramics were non-magnetic material, the real and imaginary relative permeabilities of samples were regarded as 1 and 0, respectively.  $Z_{in}$  is the normalized input impedance of composite ceramics.  $c$  is the light velocity in vacuum,  $d$  is the thickness of samples, and  $f$  is the frequency of incident electromagnetic wave.

## 3 Results and discussion

### 3.1 The microstructure and phase composition

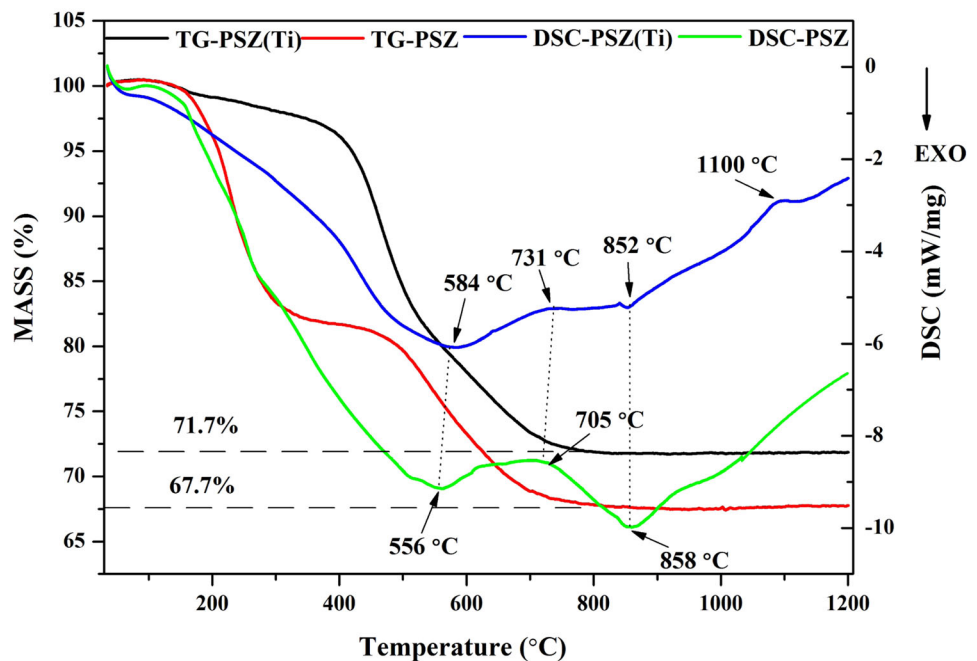
In order to understand the thermal behavior of precursor of PSZ modified by Ti (PSZ(Ti)) during the

pyrolysis and heat treatment, the TG and DSC analyses of PSZ(Ti) were conducted at temperature range from 50 °C to 1200 °C. At the same time, the same thermal behavior analysis curve of pure PSZ is also shown in the Fig. 2 as comparison. The whole thermal analysis process was protected by the Ar atmosphere. The TG curves of pure PSZ and PSZ(Ti) showed great differences between 50 °C and 800 °C. The both TG curves basically coincided during temperature range from 50 °C to 150 °C and showed almost no weight loss. The TG curve of pure PSZ precursor showed two stages weight loss in the temperature range from 150 °C to 800 °C. The first significant weight loss of pure PSZ occurred from 150 °C to 280 °C, with a decrease of 17 wt.%, which was mainly due to the uncured oligomer evaporation [6]. The second notable weight loss of pure PSZ was about 13 wt.% at temperature from 480 °C to 800 °C, which was mainly caused by cleavages of Si-H, C-H, N-H, and Si-CH<sub>3</sub> bonds in precursor and the release of hydrogen, alkenes, olefins and other gases [5]. In this process, free radicals were formed in precursor and were rearranged to form a three-dimensional network structure of amorphous phase, which realized the precursor transformation from organic to inorganic structure. However, the precursor of PSZ(Ti) showed only one stage drastic weight loss in the temperature range from 150 °C to 800 °C. From 150 °C to 410 °C, the precursor of PSZ(Ti) exhibited a

slight weight loss of about 2 wt.%. The slight weight loss of precursor of PSZ(Ti) at this temperature stage was mainly due to Si-O-Ti bonds formed in the modified precursor, which greatly reduced the evaporation of low-molecular-weight oligomer from the matrix [20, 22, 23]. The only obvious weight loss of PSZ(Ti) took place at temperature stage from 410 °C to 800 °C. In this process, the weight loss mechanism of the precursor modified by Ti was consistent with that of the pure precursor, and the slopes of TG curves of two precursors were the same. At the temperature from 800 °C to 1200 °C, there was no weight loss of two precursors, and the final ceramic yields of pure PSZ and PSZ(Ti) were 67.7 wt.% and 71.7 wt.%, respectively. From the TG analysis of two kinds of precursors above, it can be concluded that introduction of Ti in PSZ could greatly promote the crosslinking of oligomer in the precursor and finally improve the ceramic yield.

The DSC curves of two kinds of precursors showed the two similar broad exothermic peaks. The first exothermic peaks of PSZ(Ti) and PSZ were at 584 °C and 556 °C and ended at 731 °C and 705 °C, respectively. The first exothermic peak was mainly ascribed to the cleavage of the chemical bonds in precursor during the process of curing and pyrolysis [5, 6]. From the data of first exothermic peaks, the PSZ precursor modified by Ti had better thermal stability than precursor of pure PSZ during the process of

**Fig. 2** The TG-DSC curves of pure PSZ and PSZ modified by Ti



pyrolysis. The second exothermic peaks of two precursors were around 850 °C, which were mainly caused by redistribution reaction and rearrangement of chemical bond [5, 20, 24]. The DSC curve of PSZ(Ti) showed a small endothermic peak at 1100 °C, which might be due to the melting of nanotitanium [25–28].

The evolution of the crystalline phases with annealing temperature in composite ceramics were studied by XRD. It can be seen from the XRD pattern in Fig. 3 a that when the annealing temperature was below 1300 °C, there was no obvious diffraction peak in XRD pattern, indicating that the composite ceramics were amorphous. The three major diffraction peaks at 35.6°, 60.1°, and 71.8° and the weaker peak at 41.3° appeared in XRD pattern when the annealing temperature was 1400 °C, these peaks corresponded to the (111), (220), (311), and (200) planes of β-SiC, respectively (JCPDS card no.: 01-075-0254). The characteristic diffraction peaks intensity of β-SiC increased at annealing temperature of 1500 °C, which indicated that more SiC crystal particles precipitated from the matrix and crystallinity of SiC increased. At the same time, the diffraction peaks attributed to the TiC appeared at 35.9°, 41.7°, 60.4°, and 72.4° in XRD pattern (JCPDS card no.: 03-065-8417). Because diffraction peaks of SiC and TiC are so similar, the local magnification of diffraction peaks of XRD pattern at 1500 °C is show in Fig. 3b. The presence of SiO<sub>2</sub> at annealing temperature of 1500 °C might be due to the introduction of oxygen atoms of

TBT. The average grain sizes of SiC ( $D_{SiC}$ ) at 1400 °C and 1500 °C were calculated by Scherrer formula, respectively.

$$D_{SiC} = \frac{k\lambda}{\beta \cos\theta} \tag{3}$$

where the  $k$  and  $\lambda$  are Scherrer constant and X-ray wavelength, respectively.  $\beta$  is the width in radians at half maximum intensity of SiC diffraction peak.  $\theta$  is the diffraction angle of SiC. The  $D_{SiC}$  of sample at annealing temperature of 1400 °C and 1500 °C was 34.9 nm and 59.9 nm respectively, which means the crystallinity of SiC increased with the increase of annealing temperature.

However, the free carbon phase which has a great influence on microwave absorbing properties of the composite ceramics was not found in XRD patterns. Raman spectra is a very effective and sensitive method to study the transition from amorphous carbon to graphitization [29]. The Raman spectra of TiC/SiC/SiCN composite ceramics annealed at different temperatures are shown in Fig. 4a. There are two characteristic peaks of free carbon called D peak and G peak in every Raman spectrum of composite ceramics at different temperature. D peak and G peak always locate at around 1350 cm<sup>-1</sup> and 1580 cm<sup>-1</sup>, respectively. The G peak is due to stretching vibration of sp<sup>2</sup> hybrid carbon electron pairs. Any form of sp<sup>2</sup> hybridization of carbon can cause the G peak in Raman spectrum. D peak is related to the breath modes of sp<sup>2</sup> of carbon atom in the six-ring structure,

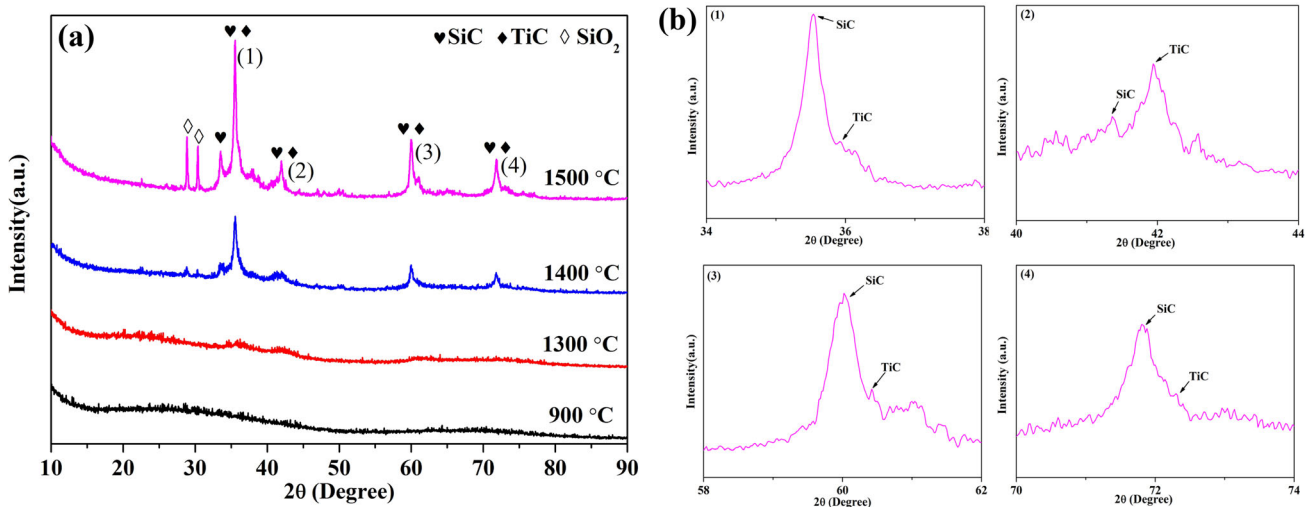


**Fig. 3** The XRD patterns of the TiC/SiC/SiCN composite ceramics annealed at different temperatures (a) and local magnification of diffraction peaks of XRD pattern at 1500 °C (b)

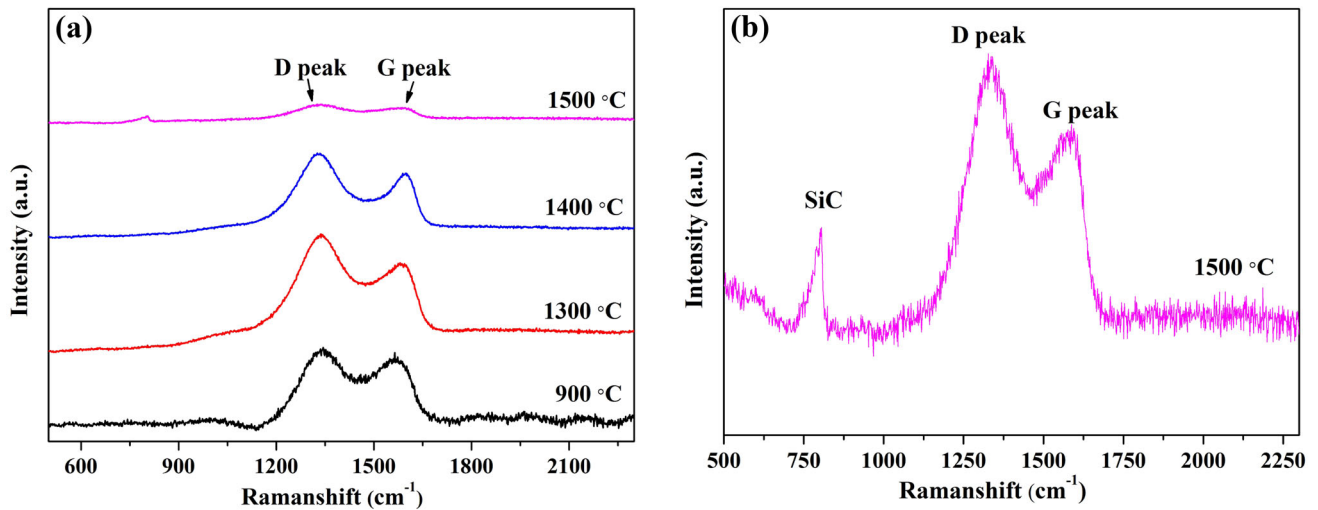


**Fig. 4** Raman spectra of the TiC/SiC/SiCN composite ceramics annealed at different temperatures (a) and Raman spectra magnification of composite ceramics annealed at 1500 °C (b)

**Table 1** Raman spectroscopy fitting curve data of TiC/SiC/SiCN composite ceramics

Samples	D peak position (cm <sup>-1</sup> )	FWHM <sub>D</sub>	G peak position (cm <sup>-1</sup> )	FWHM <sub>G</sub>	$I_D/I_G$	$L_a$ (nm)
900 °C	1346	179	1557	141	1.15	1.45
1300 °C	1338	167	1584	104	1.42	1.61
1400 °C	1330	147	1594	97	1.40	1.60
1500 °C	1338	152	1584	71	1.21	1.48

which represents the existence of disordered structure of carbon. The D peak and G peak in Raman spectra were fitted by Lorentzian function and Breit-Wigner-Fano (BWF) function, respectively [30, 31]. The data of fitting peaks are listed in Table 1. At the same time, the ratio intensity of D peak and G peak ( $I_D/I_G$ ) is usually used as an indicator of the defect concentration, and widely applied to estimate the size of graphite nanograins ( $L_a$ ) [32–34]. When the  $L_a$  is less than 2 nanometers, the square of  $L_a$  is proportional to  $I_D/I_G$  and can be calculated by formula (4). The  $I_D/I_G$  is peak height ratio, and coefficient  $c(\lambda) \approx 0.0055$  ( $\lambda=514$  nm).

$$\frac{I_D}{I_G} = c(\lambda)L_a^2 \quad (4)$$

when the annealing temperature was lower than 1400 °C, with the increase of annealing temperature, the intensities of D peak and G peak increased, the full width at half maximum (FWHM) of D peak and G peak decreased, the position of D peak moved slightly to low wave number [29, 32], the position of

G peak moved to high wave number, the size of graphite nanograins ( $L_a$ ) increased from 1.45 nm to 1.60 nm. All the above phenomena indicated that more  $sp^2$  hybrid carbon with six-ring structure was formed, and amorphous carbon gradually transformed into nano-graphitized carbon. However, when the annealing temperature was 1500 °C, the intensities, FWHM, position of the D peak and G peak changed in the opposite direction. The size of graphite nanograins ( $L_a$ ) was reduced to 1.48 nm. At the same time, it can be seen from Fig. 4b that the SiC peak appeared at 798 cm<sup>-1</sup> in Raman spectrum [20, 35]. The appearance of SiC may be due to the reaction of free carbon with Si-O bonds in the samples to form crystallized SiC [20]. The evolution of Raman spectrum data at annealing temperature of 1500 °C indicated that a large amount of free carbon was consumed in the composite ceramics.

The morphologies of TiC/SiC/SiCN composite ceramics annealed at different temperatures are shown in the SEM images of Fig. 5. It can be seen from the Fig. 5a and b that plenty open pores existed

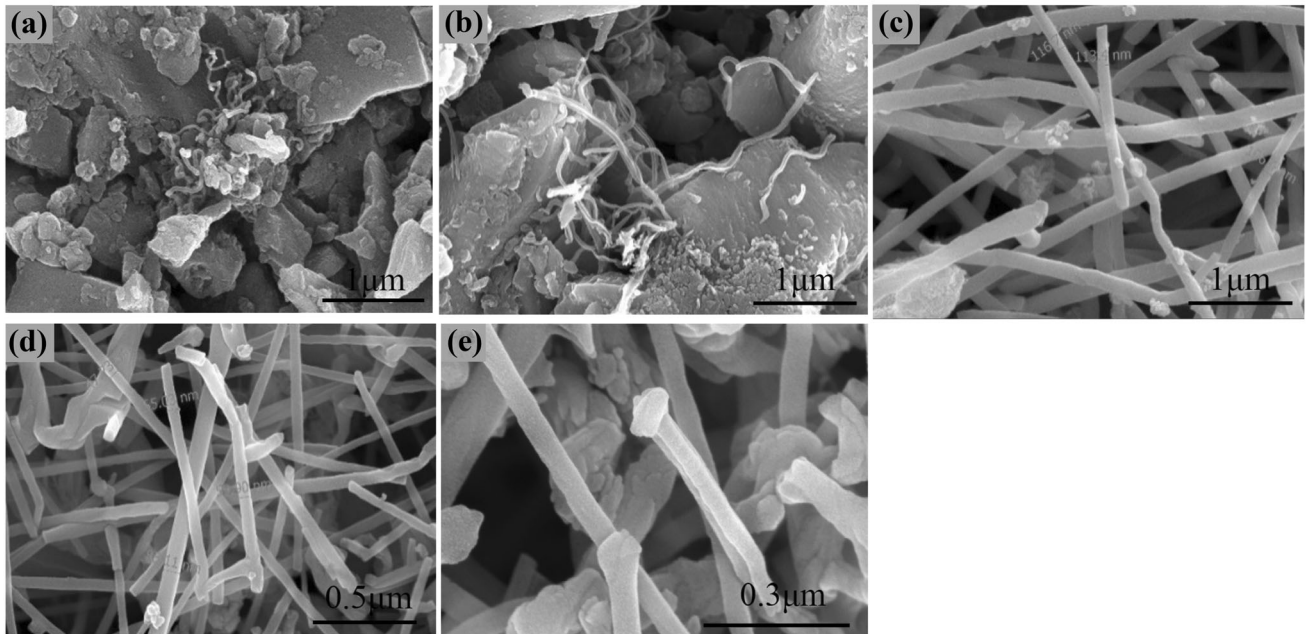


**Fig. 5** SEM images of the TiC/SiC/SiCN composite ceramics annealed at **a** 900 °C, **b** 1300 °C, **c** 1400 °C, and **d** 1500 °C and **e** magnified image of the SiC nanowires

between ceramics particles, and there were a small number of nanowires in the pores. When the annealing temperature reached 1400 °C, a large number of nanowires with the diameter of about 106–117 nm were formed in the composite ceramics. However, the diameter of nanowires was reduced to 47–84 nm at annealing temperature of 1500 °C. It can be clearly observed in Fig. 5e that there were irregular particles on the top of nanowires. The diameter of nanoparticles was slightly larger than that of nanowires. Energy-dispersive spectroscopy (EDS) analysis showed that the nanowires in composite ceramics were SiC nanowires, and the nanoparticles on the top of nanowires were titanium alloy particles. The irregular spherical titanium alloy particles on the top of nanowires indicated that the formation of SiC nanowires was attributed to the vapor-liquid-solid mechanism [36].

Further, TEM was carried out to reveal the microstructure of composite ceramics annealed at 1500 °C in Fig. 6a. There were two different nanocrystals embedded in the amorphous SiCN matrix, which were marked by green and red circles, respectively. High-resolution transmission electron microscopy (HRTEM) and selected-area electron diffraction (SAED) were used to characterize the two

different nanocrystals. Figure 6b presents the HRTEM image of SiC in circle of Fig. 6a. The crystal interplanar spacing in the image was about 0.25 nm, which corresponded to the (111) plane of  $\beta$ -SiC. The diffraction rings pattern shown in the upper right inset indicated that there were polycrystalline SiC nanocrystals in green circle region. The size of SiC nanograins in green circle was about 60 nm, which was consistent with the size calculated by Scherrer formula. The HRTEM image and SAED pattern of TiC show in the Fig. 6c. The crystal interplanar spacing with 0.22 nm corresponded to the (200) plane of TiC. The SEAD pattern in the upper right corner inset showed that there was single-crystalline TiC in red circle region.

According to the above analysis and characterization, the microstructure evolution of TiC/SiC/SiCN composite ceramics can be summarized as follows. Titanium was successfully introduced into the precursor by the condensation reaction of Si-H bonds of PSZ and butoxy group of TBT at 60 °C. After pyrolysis at 900 °C, the chemical bonds in precursors were broken and rearranged. The precursor changed from organic to inorganic microstructure. The composite ceramics were amorphous when the annealing temperature was below 1300 °C. At 1400 °C, SiC

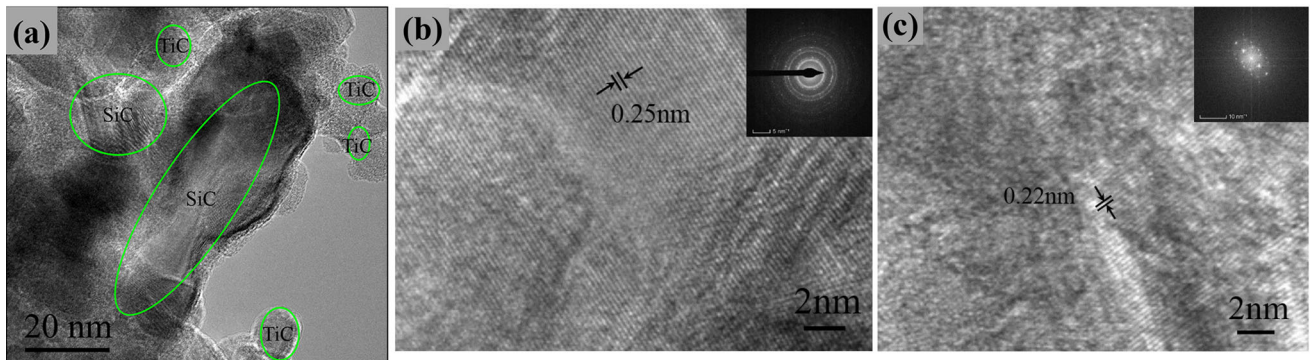


**Fig. 6** TEM images of the TiC/SiC/SiCN composite ceramics annealed at **a** 1500 °C and HRTEM images of SiC (**b**) and TiC (**c**)

nanograins began to precipitate from the matrix, and a large number of SiC nanowires were formed in the pores of ceramics. The precipitation temperature of PDCs-SiCN ceramics modified by Ti was much lower than that of pure PDCs-SiCN [6]. There are two main reasons to promote the precipitation of SiC from PDCs-SiCN(Ti). Firstly, titanium nanograins formed during the heat treatment as heterogeneous interfaces greatly reduced Gibbs free energy of SiC precipitated from the matrix. Secondly, because of small size of titanium nanograins, titanium nanograins melted into droplets at lower temperature. The molten titanium alloy droplets acted as catalyst to absorb small gaseous molecules such as SiO and CO produced by fracture and rearrangement of chemical bonds from matrix during the process of heat treatment. When the Si and C atoms were saturated in the alloy droplets, SiC nanowires precipitated from the alloy droplets. When the annealing temperature rose to 1500 °C, more SiC precipitated from the matrix. However, due to the reaction between titanium and free carbon to form TiC, the catalytic effect of titanium was weakened and growth of SiC nanowires was restricted, resulting in the reduction of the size of SiC nanowires. At the same time, because the carbothermal reduction reaction usually started at 1500 °C in Ar atmosphere, a large amount of free carbon in the matrix might also be greatly consumed by carbothermal reduction reaction. Finally, PDCs-SiCN composite ceramics modified by Ti with a microstructure containing multi-phases and multiple nano heterogeneous interfaces were obtained.

### 3.2 Dielectric and microwave absorption properties of the TiC/SiC/SiCN composite ceramics

The complex permittivity of composite ceramics is a key parameter for the non-magnetic materials to predict the absorbing properties of materials, and it is closely related to the microstructure evolution of composite ceramics. The complex permittivity of samples with dimensions of 22.86 mm × 10.16 mm × 2 mm was measured by waveguide method with a vector network analyzer. Figure 7a-c present the real part ( $\epsilon'$ ), the imaginary part ( $\epsilon''$ ) of complex permittivity, and tangent loss ( $\tan\delta = \epsilon''/\epsilon'$ ) of composite ceramics with annealing temperature in X band. It can be concluded that the complex permittivity of composite ceramics was greatly influenced by annealing temperature. When the annealing temperature was below 1300 °C,  $\epsilon'$ ,  $\epsilon''$ , and  $\tan\delta$  almost remained unchanged, and the average value of  $\epsilon'$ ,  $\epsilon''$ , and  $\tan\delta$  was about 4.1, 0, and 0, respectively. The composite ceramics annealed below 1300 °C had almost no dielectric loss, showing the characteristics of electromagnetic wave transmission, which was consistent with amorphous microstructure of composite ceramics. When the annealing temperature reached 1400 °C, the complex permittivity of composite ceramics increased greatly, the average value of  $\epsilon'$ ,  $\epsilon''$ , and  $\tan\delta$  were about 12.5, 10.4, and 0.83, respectively. The significant increase of complex permittivity of composite ceramics was due to precipitation of a large amount of SiC nanograins, SiC nanowires, and free carbon in matrix. However, the average value of  $\epsilon'$ ,  $\epsilon''$ , and  $\tan\delta$  decreased to 11.6, 5.9, and 0.51 at annealing temperature of 1500 °C, as free



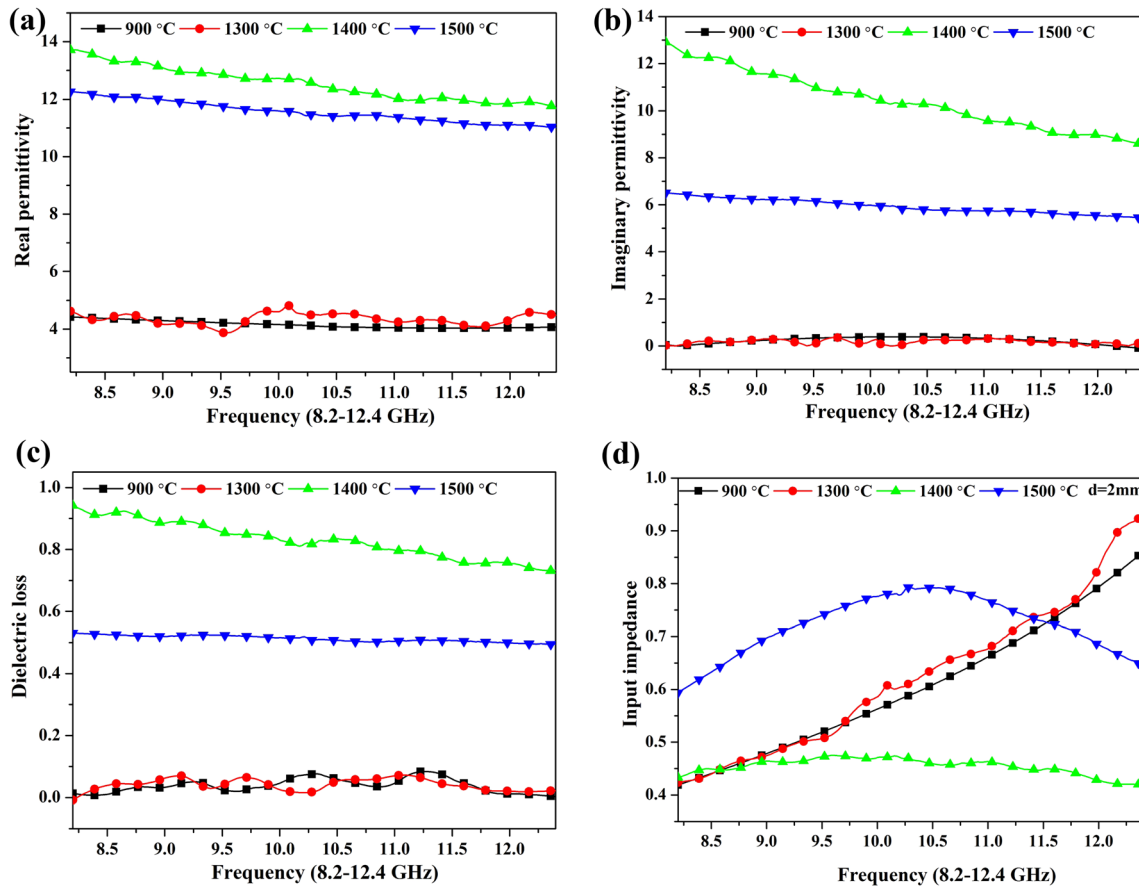


**Fig. 7** **a** Real part, **b** imaginary part permittivity, **c** loss tangents, and **d** input impedance of the TiC/SiC/SiCN composite ceramics annealed at different temperatures in X band

carbon was greatly consumed by titanium to produce TiC and the formation of SiC was restricted. The normalized input impedances of composite ceramics at thickness of 2 mm were calculated by formula (2) and shown in Fig. 7d. According to the impedance matching principle, when normalized input impedance satisfies  $|z - 1| = 0$ , the electromagnetic wave can enter the material completely without any reflection on the surface of material. Therefore, in order to obtain good absorbing performance, the normalized input impedance should be as close as possible to 1. It can be seen from Fig. 7d that input impedance of the sample annealed at 1500 °C was closer to 1 than that of other samples annealed at other temperature. Although the sample annealed at 1400 °C had higher complex permittivity and dielectric loss, its impedance matching was poor and would cause large reflection. The input impedances of samples annealed at 900 °C and 1300 °C were close to 1 from 11.5 GHz to 12.4 GHz, but the dielectric

losses of two samples were too low to have good microwave absorbing performance.

The RL of samples with thickness of 2 mm at different annealing temperatures was calculated by formula (1) and shown in Fig. 8a. The average RL values of samples annealed at 900 °C and 1300 °C were about  $-0.1$  dB, which meant that samples almost had no absorbing properties. This was because the composite ceramics were amorphous and dielectric loss was almost zero when annealing temperature was below 1300 °C. When the annealing temperature reached 1400 °C, the average RL value of sample was  $-7.7$  dB and EAB is 0 although the sample had high complex permittivity and dielectric loss. The poor absorbing performance was due to the impedance mismatch caused by the precipitation of too much SiC nanograins, nanowires, and free carbon. Abundant conductive phases caused electromagnetic wave reflection on the surface of sample. The average RL value of sample annealed at 1500 °C was  $-11.5$  dB. The minimum RL was  $-16.4$  dB at

11.2 GHz and EAB reaches 2.6 GHz. The enhanced microwave absorbing performance of composite ceramics annealed at 1500 °C was attributed to two factors. Firstly, the consumption of free carbon made composite ceramics have better impedance matching, greatly reducing the reflection of electromagnetic wave, which provided a prerequisite for good microwave absorbing performance. Secondly, when annealing temperature reaches 1500 °C, a large number of nanophase was formed in the composite ceramics, including TiC nanograins, SiC nanograins, and nanowires, nanocrystalline graphite and so on. The high polarization interface loss caused by various nanophases made the composite ceramics have good microwave absorbing performance. The RL of composite ceramics annealed at 1500 °C with different thickness is shown in Fig. 8b. The minimum value of RL gradually moved toward low frequency with the increase of thickness of samples. The evolution of minimum RL with sample thickness was due to interference cancelation between the electromagnetic reflection wave on the sample surface and bottom when the thickness of sample was an odd multiple of quarter electromagnetic wave. The minimum RL of samples was  $-17.1$  dB at the thickness of 1.9 mm, and the maximum EAB of RL was 3.2 GHz from 9.2 GHz to 12.4 GHz when the thickness of sample was 2.1 mm.

The outstanding microwave absorbing performance is due to the formation of multi-nanophases and multiple nano heterogeneous interfaces to attenuate the electromagnetic wave energy propagated in composite ceramics. There are four main electromagnetic wave absorption mechanisms in the composite ceramics. The schematic of

electromagnetic wave absorption mechanisms in the composite ceramics is shown in Fig. 9.

Firstly, due to the existence of a large number of nanophases in composite ceramics and the high specific surface area of nano phase, a large amount of heterogeneous interfaces and permittivity gradient are generated in composite ceramics. When electromagnetic wave propagates in the composite ceramics, the induced charge will accumulate, dissipate, and oscillate between heterogeneous interfaces. When the induced charges between heterogeneous interfaces cannot keep up with the oscillation of the electromagnetic wave, a high interface polarization loss is produced [37]. Secondly, previous researches have shown that the defects in SiCN composite ceramics are mainly the dangling bond defects of carbon, and there are no defects related with Si [38, 39]. Under the action of electromagnetic wave, the carbon defects in composite ceramics will form dipoles. The dipoles will rotate with electromagnetic wave oscillation. When the dipoles rotate lag electromagnetic wave oscillation, the microwave energy is consumed by dipole relaxation loss. Thirdly, a large number of nanophases precipitated from the matrix, including nanocrystalline SiC, TiC, graphite and SiC nanowires in the pores, are easy to form local conductive networks in matrix. Induced microcurrent caused by electromagnetic wave conducts in the networks, converting electromagnetic energy into heat energy to form conductivity loss [40]. Moreover, SiC nanowires are also an important factor in electromagnetic wave loss. The SiC nanowires randomly distributed in matrix acts as microwave receiving antennas, which can induce the vibrating microcurrent in nanowires. The microcurrent is introduced and

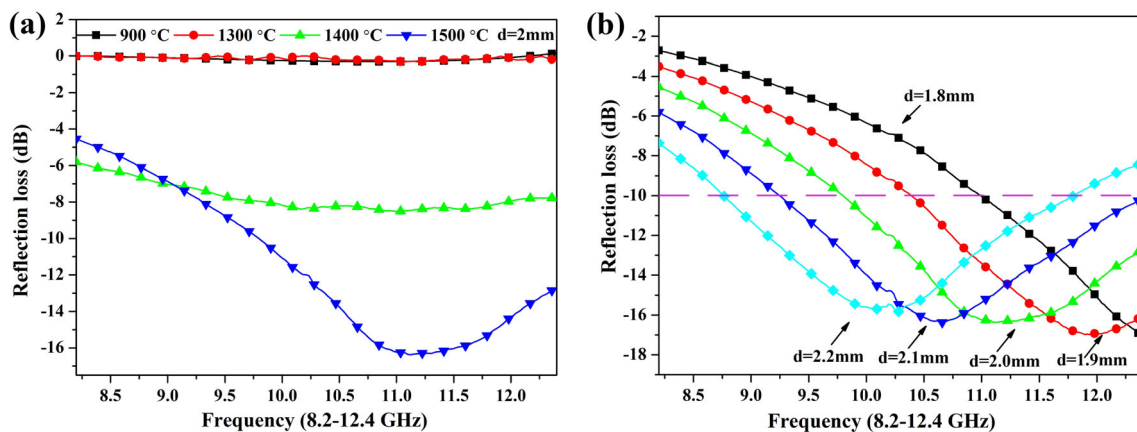
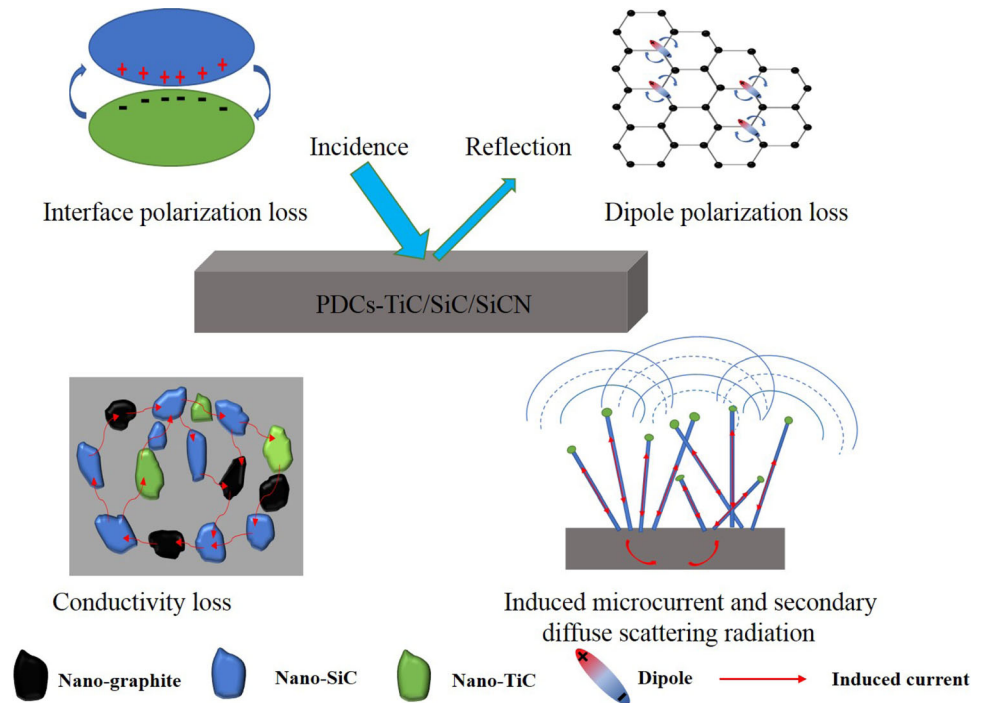


**Fig. 8** **a** RL calculated at different temperatures and **b** RL at different thicknesses at the annealing temperature of 1500 °C in X band

**Fig. 9** Schematic of electromagnetic wave absorption mechanisms in the composite ceramics



exhausted in the local conductive networks in matrix. At the same time, according to the theory of antenna, the microcurrent in antennas will also excite alternating electromagnetic field around SiC nanowires, causing electromagnetic omni direct radiation. However, the microwave secondary radiation generated by SiC nanowires makes electromagnetic wave change from directional to diffuse scattering because of the random distribution of SiC nanowires in matrix, which will greatly attenuate the energy of electromagnetic wave [41–45].

#### 4 Conclusions

PDCs-TiC/SiC/SiCN composite ceramics were successfully fabricated by the pyrolysis of solid PSZ modified by Ti. Compared with composite ceramics prepared by pure PSZ, the introduction of Ti in precursor greatly reduced the precipitation temperature of SiC nanograins from the SiCN composite ceramics. When annealing temperature reached 1500 °C, PDCs-TiC/SiC/SiCN composite ceramics formed a microstructure containing abundant nanophases and nanostructures (including TiC nanocrystals, SiC nanocrystals and nanowires, graphite nanocrystals and so on). Owing to the formation of permittivity gradient between varied nanodielectric loss phases

and appropriate carbon content in matrix, PDCs-TiC/SiC/SiCN composite ceramics had good input impedance matching and EM wave absorbing property in X band. The minimum RL of samples was – 17.1 dB at the thickness of 1.9 mm, and the maximum EAB of RL was 3.2 GHz when the thickness of sample was 2.1 mm. Meanwhile, previous researches have shown that the growth of SiC nanocrystals can be significantly restricted when a large amount of TiC nanograins are generated in composite ceramics. Due to pinning and dispersion strengthening, the high-temperature mechanical properties, oxidation, and creep resistance of PDCs-TiC/SiC/SiCN composite ceramics are also greatly improved [18, 46–49]. So the excellent microwave absorbing performance of PDCs-TiC/SiC/SiCN composite ceramics will make it possible to become a promising structural and microwave absorbing integration material.

#### Acknowledgements

This work is financially supported by the National Natural Science Foundation of China (51821091 and 51902257), the National Science Fund for Distinguished Young Scholars (51725205), and the 111 Project (B08040). We would like to thank my mentor professor Xiaowei Yin for his guidance and help.

## References

- X. Yin, L. Kong, L. Zhang, L. Cheng, N. Travitzky, P. Greil, Electromagnetic properties of Si–C–N based ceramics and composites. *Int. Mater. Rev.* **59**(6), 1743–2804 (2014)
- W. Duan, X. Yin, Q. Li, L. Schlier, P. Greil, A review of absorption properties in silicon-based polymer derived ceramics. *J. Eur. Ceram. Soc.* **36**(15), 3681–3689 (2016)
- C. Beall, E. Delzell, P. Cole, I. Brill, Brain tumors among electronics industry workers. *Epidemiology* **7**(2), 125–130 (1996)
- P. Colombo, G. Mera, R. Riedel, G.D. Soraru, Polymer-derived ceramics: 40 years of research and innovation in advanced ceramics. *J. Am. Ceram. Soc.* **93**(7), 1805–1837 (2010)
- Q. Li, X. Yin, W. Duan, L. Cheng, L. Zhang, Improved dielectric properties of PDCs-SiCN by in-situ fabricated nano-structured carbons. *J. Eur. Ceram. Soc.* **37**(4), 1243–1251 (2017)
- Q. Li, X. Yin, W. Duan, B. Hao, L. Kong, X. Liu, Dielectric and microwave absorption properties of polymer derived SiCN ceramics annealed in N<sub>2</sub> atmosphere. *J. Eur. Ceram. Soc.* **34**(3), 589–598 (2014)
- J. Xue, X. Yin, L. Cheng, Induced crystallization behavior and EMW absorption properties of CVI SiCN ceramics modified with carbon nanowires. *Chem. Eng. J.* **378**, 122213 (2019)
- F. Ye, L. Zhang, X. Yin, X. Liu, Y. Liu, L. Cheng, SiCN-based composite ceramics fabricated by chemical vapor infiltration with excellent mechanical and electromagnetic properties. *Mater. Lett.* **111**, 169–172 (2013)
- H. Wei, X. Yin, X. Li, M. Li, X. Dang, L. Zhang, L. Cheng, Controllable synthesis of defective carbon nanotubes/Sc<sub>2</sub>Si<sub>2</sub>O<sub>7</sub> ceramic with adjustable dielectric properties for broadband high-performance microwave absorption. *Carbon* **147**, 276–283 (2019)
- Y. Zhang, X. Yin, F. Ye, L. Kong, Effects of multi-walled carbon nanotubes on the crystallization behavior of PDCs-SiBCN and their improved dielectric and EM absorbing properties. *J. Eur. Ceram. Soc.* **34**(5), 1053–1061 (2014)
- H. Pan, X. Yin, J. Xue, L. Chen, L. Zhang, In-situ synthesis of hierarchically porous and polycrystalline carbon nanowires with excellent microwave absorption performance. *Carbon* **107**, 36–45 (2016)
- W. Duan, X. Yin, F. Ye, Q. Li, M. Han, X. Liu, M. Han, Y. Cai, Synthesis and EMW absorbing properties of nano SiC modified PDC-SiOC. *J. Mater. Chem. C* **4**(25), 5962–5969 (2016)
- M. Han, X. Yin, W. Duan, S. Ren, L. Zhang, L. Cheng, Hierarchical graphene/SiC nanowire networks in polymer-derived ceramics with enhanced electromagnetic wave absorbing capability. *J. Eur. Ceram. Soc.* **36**(11), 2695–2703 (2016)
- L. Kong, C. Wang, X. Yin, X. Fan, W. Wang, J. Huang, Electromagnetic wave absorption properties of a carbon nanotube modified by a tetrapyridinoporphyrazine interface layer. *J. Mater. Chem. C* **5**, (2017)
- H. Wu, L. Wang, S. Guo, Y. Wang, Z. Shen, Electromagnetic and microwave-absorbing properties of highly ordered mesoporous carbon supported by gold nanoparticles. *Mater. Chem. Phys.* **133**, 965–970 (2012)
- L. Kong, X. Yin, M. Han, X. Yuan, Z. Hou, F. Ye, L. Zhang, L. Cheng, Z. Xu, J. Huang, Macroscopic bioinspired graphene sponge modified with in-situ grown carbon nanowires and its electromagnetic properties. *Carbon* **111**, 94–102 (2017)
- L. Kong, X. Yin, H. Xu, X. Yuan, T. Wang, Z. Xu, J. Huang, R. Yang, H. Fan, Powerful absorbing and lightweight electromagnetic shielding CNTs/RGO composite. *Carbon* **145**, 61–66 (2019)
- H. Wu, L. Wang, Y. Wang, S. Guo, S. Guo, Z. Shen, Enhanced microwave performance of highly ordered mesoporous carbon coated by Ni<sub>2</sub>O<sub>3</sub> nanoparticles. *J. Alloy. Compd.* **525**, 82–86 (2012)
- K. Luo, X. Yin, F. Ye, Q. Li, L. Zhang, L. Cheng, Electromagnetic wave absorption properties of ZnO-based materials, modified with ZnAl<sub>2</sub>O<sub>4</sub> nanograins. *J. Phys. Chem. C* **117**(5), 2135–2146 (2013)
- Z. Yu, J. Zhan, C. Zhou, L. Yang, R. Li, H. Xia, Synthesis and characterization of SiC(Ti) ceramics derived from a hybrid precursor of titanium-containing polycarbosilane. *J. Inorg. Organomet. P* **21**(3), 412–420 (2011)
- T. Ishikawa, T. Yamamura, K. Okamura, Production mechanism of polytitanocarbosilane and its conversion of the polymer into inorganic materials. *J. Mater. Sci.* **27**(24), 6627–6634 (1992)
- Y.C. Song, Y. Hasegawa, S.J. Yang, M. Sato, Ceramic fibres from polymer precursor containing Si-O-Ti bonds part I: the formation mechanism and the pyrolysis of the polymer. *J. Mater. Sci.* **23**, 1911–1920 (1988)
- Y. Hasegawa, C.X. Feng, Y.C. Song, Z.L. Tan, Ceramic fibres from polymer precursor containing Si-O-Ti bonds. Part II synthesis of the various types of ceramic fibres. *J. Mater. Sci.* **26**, 3657–3664 (1991)
- M.A. Schiavon, G.D. Soraru, I. Valeria, P. Yoshida, Synthesis of a polycyclic silazane network and its evolution to silicon carbonitride glass. *J. Non-Cryst. Solids* **304**(1), 76–83 (2002)
- H.B. Liu, J.A. Ascencio, M. Perez-Alvarez, M.J. Yacamán, Melting behavior of nanometer sized gold isomers. *Surf. Sci.* **491**, 88–98 (2001)

26. K. Lu, Z.H. Jin, Melting and superheating of low-dimensional materials. *Curr. Opin. Solid St. M.* **5**(1), 39–44 (2001)
27. S.S. Ryu, Y.D. Kim, I.H. Moon, Dilatometric analysis on the sintering behavior of nanocrystalline W-Cu prepared by mechanical alloying. *J. Alloy. Compd.* **335**(1), 233–240 (2002)
28. H.W. Sheng, Z.Q. Hu, K. Lu, Melting and freezing behaviors of Pb nanoparticles embedded in an Al matrix. *Nanostruct. Mater.* **9**(1), 661–664 (1997)
29. R.O. Dillon, J.A. Woollam, Use of Raman scattering to investigate disorder and crystallite formation in as-deposited and annealed carbon films. *Phys. Rev. B* **29**(6), 3482–3489 (1984)
30. A.C. Ferrari, J. Robertson, Resonant Raman spectroscopy of disordered, amorphous, and diamondlike carbon. *Phys. Rev. B* **64**(7), 075414 (2001)
31. A.C. Ferrari, J. Robertson, Interpretation of Raman spectra of disordered and amorphous carbon. *Phys. Rev. B* **61**(20), 14095–14107 (2000)
32. A.C. Ferrari, Raman spectroscopy of graphene and graphite: Disorder, electron–phonon coupling, doping and nonadiabatic effects. *Solid State Commun.* **143**, 47–57 (2007)
33. P. Mallet-Ladeira, P. Puech, C. Toulouse, M. Cazayous, N. Ratel-Ramond, P. Weisbecker, G.L. Vignoles, M. Monthieux, A Raman study to obtain crystallite size of carbon materials: A better alternative to the Tuinstra–Koenig law. *Carbon* **80**, 629–639 (2014)
34. M.R. Ammar, N. Galy, J.N. Rouzaud, N. Toulhoat, C.E. Vaudey, P. Simon, N. Moncoffre, Characterizing various types of defects in nuclear graphite using Raman scattering: Heat treatment, ion irradiation and polishing. *Carbon* **95**, 364–373 (2015)
35. Z. Yu, H. Min, J. Zhan, L. Yang, Preparation and dielectric properties of polymer-derived SiCTi ceramics. *Ceram. Int.* **39**, 3999–4007 (2013)
36. R.S. Wagner, W.C. Ellis, Vapor-liquid-solid mechanism of single crystal growth. *Appl. Phys. Lett.* **4**(5), 89–90 (1964)
37. H. Xu, X. Yin, X. Fan, Z. Tang, Z. Hou, M. Li, X. Li, L. Zhang, L. Cheng, Constructing a tunable heterogeneous interface in bimetallic metal-organic frameworks derived porous carbon for excellent microwave absorption performance. *Carbon* **148**, 421–429 (2019)
38. T.J. McMahon, Y. Xiao, Electron spin resonance study of the dangling bond in amorphous Si and porous Si. *Appl. Phys. Lett.* **63**(12), 1657–1659 (1993)
39. A.A. Konchits, M.Y. Valakh, B.D. Shanina, S.P. Kolesnik, I.B. Yanchuka, Effects of ion implantation on electron centers in hydrogenated amorphous carbon films. *J. Appl. Phys.* **93**(10), 5905–5910 (2003)
40. H. Wei, X. Yin, F. Jiang, Z. Hou, L. Cheng, L. Zhang, Optimized design of high-temperature microwave absorption properties of CNTs/Sc<sub>2</sub>Si<sub>2</sub>O<sub>7</sub> ceramics. *J. Alloy. Compd.* **823**, 153864 (2020)
41. Y. Chen, M. Cao, T. Wang, Q. Wan, Microwave absorption properties of the ZnO nanowire-polyester composites. *Appl. Phys. Lett.* **84**(17), 3367–3369 (2004)
42. R. Zhuo, L. Qiao, H. Feng, J. Chen, D. Yan, Z. Wu, P. Yan, Microwave absorption properties and the isotropic antenna mechanism of ZnO nanotrees. *J. Appl. Phys.* **104**(9), 94101 (2008)
43. M. Cao, X. Shi, X. Fang, H. Jin, Z. Hou, W. Hou, Y. Chen, Microwave absorption properties and mechanism of cage-like ZnO/SiO<sub>2</sub> nanocomposites. *Appl. Phys. Lett.* **91**(20), 203110 (2007)
44. X. Fang, M. Cao, X. Shi, Z. Hou, W. Song, J. Yuan, Microwave responses and general model of nanotetranedle ZnO: Integration of interface scattering, microcurrent, dielectric relaxation, and microantenna. *J. Appl. Phys.* **107**(5), 54304 (2010)
45. X. Fang, X. Shi, M. Cao, J. Yuan, Micro-current attenuation modeling and numerical simulation for cage-like ZnO/SiO<sub>2</sub> nanocomposite. *J. Appl. Phys.* **104**(9), 96101 (2008)
46. T. Yamamura, T. Ishikawa, M. Shibuya, T. Hisayuki, Development of a new continuous Si-Ti-C-O fibre using an organometallic polymer precursor. *J. Mater. Sci.* **23**, 2589–2594 (1988)
47. P. Amorós, D. Beltrán, C. Guillem, J. Latorre, Synthesis and characterization of SiC/MC/C ceramics (M = Ti, Zr, Hf) starting from totally non-oxidic precursors. *Chem. Mater.* **14**(4), 1585–1590 (2002)
48. L.P. Zawada, T. Ishikawa, Mechanical behavior of a Si-Ti-C-O fiber-bonded ceramic material. *Key Eng. Mater.* **164–165**, 245–248 (1998)
49. J. Hapke, G. Ziegler, Synthesis and pyrolysis of liquid organometallic precursors for advanced Si-Ti-C-N composites. *Adv. Mater.* **7**(4), 380–384 (1995)

**Publisher's note** Springer Nature remains neutral with regard to jurisdictional claims in published maps and institutional affiliations.